TOXICOLOGICAL SCIENCES **92(1)**, 174–185 (2006)
doi:10.1093/toxsci/kfj197
Advance Access publication April 12, 2006

Correlating Nanoscale Titania Structure with Toxicity: A Cytotoxicity and Inflammatory Response Study with Human Dermal Fibroblasts and Human Lung Epithelial Cells

Christie M. Sayes,*,[1] Rajeev Wahi,* Preetha A. Kurian,* Yunping Liu,* Jennifer L. West,†,‡ Kevin D. Ausman,‡ David B. Warheit,§ and Vicki L. Colvin*,‡

Department of Chemistry, †Department of Bioengineering, and ‡Center for Biological and Environmental Nanotechnology, Rice University, Houston, Texas 77005; and §DuPont Haskell Lab, Newark, Delaware 19714

Received December 19, 2005; accepted April 7, 2006

Nanocrystalline titanium dioxide (nano-TiO_2) is an important material used in commerce today. When designed appropriately it can generate reactive species (RS) quite efficiently, particularly under ultraviolet (UV) illumination; this feature is exploited in applications ranging from self-cleaning glass to low-cost solar cells. In this study, we characterize the toxicity of this important class of nanomaterials under ambient (e.g., no significant light illumination) conditions in cell culture. Only at relatively high concentrations (100 μg/ml) of nanoscale titania did we observe cytotoxicity and inflammation; these cellular responses exhibited classic dose-response behavior, and the effects increased with time of exposure. The extent to which nanoscale titania affected cellular behavior was not dependent on sample surface area in this study; smaller nanoparticlulate materials had effects comparable to larger nanoparticle materials. What did correlate strongly to cytotoxicity, however, was the phase composition of the nanoscale titania. Anatase TiO_2, for example, was 100 times more toxic than an equivalent sample of rutile TiO_2. The most cytotoxic nanoparticle samples were also the most effective at generating reactive oxygen species; *ex vivo* RS species generation under UV illumination correlated well with the observed biological response. These data suggest that nano-TiO_2 samples optimized for RS production in photocatalysis are also more likely to generate damaging RS species in cell culture. The result highlights the important role that *ex vivo* measures of RS production can play in developing screens for cytotoxicity.

Key Words: **nanoscale titanium dioxide; titania; nano-TiO_2 particles; cytotoxicity; inflammation mediators; photocatalysis; reactive oxygen species.**

The objective of this study is to establish how the chemical properties of titania nanocrystals correlate to their *in vitro* toxicological effects. Nanoparticles offer a particularly interesting system for establishing such correlations; some of their properties are smoothly varying with both particle size and shape, and modern synthetic methods can produce highly monodisperse particles of well-defined phase composition (Katari *et al.*, 1994; Murray *et al.*, 1993; Trentler *et al.*, 1999; Yu *et al.*, 2004). These highly uniform samples have been crucial to the identification of size tunable properties in nanoscale systems, and this knowledge has in turn driven applications of nanoparticles in technologies as diverse as cancer phototherapy and self-cleaning glass (Alivisatos, 1996; Chang *et al.*, 2005; Colvin, 2003; Hirsch *et al.*, 2003; Parkin and Palgrave, 2005; Martin, 1994; Murray *et al.*, 1993). This high level of material control now also enables the detailed examination of how the size, shape, and phase-dependent properties of nanoparticles affect biological systems (Colvin, 2003; Fortner *et al.*, 2005; Vogler, 1998). An understanding of these relationships will permit nanoscale scientists and engineers to create environmentally friendly and biologically relevant nanomaterials. In addition, if chemical properties can be established as a strong predictor for toxicological behavior, then *ex vivo* tests become powerful initial screens for the design of low-toxicity nanomaterials.

In this study, we exploit state-of-the-art methods in nanochemistry to generate a set of nanocrystalline titanium dioxide (nano-TiO_2) samples of controlled phase composition and rely on *in vitro* cytotoxicity assays to compare their biological effects. The production of nanocrystalline titania in liquid phase reactions has been of great interest over the past decade (Chemseddine and Mortiz, 1999; Trentler *et al.*, 1999). In this work, we use hydrothermal methods to generate nano-TiO_2 samples of varying phase composition. Surface coatings were intentionally eliminated in these experiments not only because of our focus on phase composition and but also because of the widespread use of uncoated materials in commerce (http://azonano.com/). As a result, the nanoparticles exist in soft aggregates (a porous aggregate with high moisture absorption) in biological media. The biological effects are examined using *in vitro* studies in two human cell lines. Cytotoxicity screens are emerging as simple and cost-effective ways to evaluate the

[1] To whom correspondence should be addressed. Fax: 302-366-5207. E-mail: christie.m.sayes@usa.dupont.com.

toxicity of these complex systems and are well suited to comparative toxicological studies of different nanoparticle systems (Kirchner *et al.*, 2005; Oberdorster *et al.*, 2005; Sayes *et al.*, 2004, 2005). In this work, we use such comparisons to further develop for the structure-function relationships for engineered nanotitania toxicology (Cai *et al.*, 1992; Gurr *et al.*, 2005; Uchino *et al.*, 2002).

We chose nano-TiO_2 for this work not only because it is already an important commercial material but also because there is extensive knowledge about how its chemical properties depend on nanoparticle phase and size (Li *et al.*, 2001; Paul and Moulik, 1997; Tadros, 1993). Anatase TiO_2 with dimensions under 100 nm is a high refractive index material with low scattering and strong absorption of ultraviolet (UV) radiation (Davis, 1992; Hashimoto *et al.*, 2000; Serpone *et al.*, 2001). This material is currently used in products such as sunscreens (Serpone *et al.*, 2001) and coatings for self-cleaning windows (Parkin and Palgrave, 2005). TiO_2, in its larger micron-scale form, is generally inert; however, nano-TiO_2 particles under illumination are strong oxidizing agents capable of reacting with a wide range of organic and biological molecules (Serpone *et al.*, 2001). Their reactivity is generally ascribed to the dissociative adsorption of water to titania surfaces; under illumination, highly reactive carriers trap onto nanotitania surfaces and facilitate the transformation of chemisorbed water into $OH^{\bullet}$. This process can be leveraged in photocatalysis where nanotitania materials are used to remove organic compounds in water (Hurum *et al.*, 2003, 2005; Parkin and Palgrave, 2005; Rajeshwar *et al.*, 2001; Serpone and Emeline, 2005; Zhang and Banfield, 1999). Interest in the use of titania in photocatalysis has driven extensive work on optimization of nanotitania samples for reactive species (RS) generation; phase composition, even more than nanoparticle size, has emerged as the key material parameter (Ding *et al.*, 2000; Linsebigler *et al.*, 1995; Ohtani and Nishimoto, 1993). This prior literature informed our choice of samples for these experiments. Our nanotitania samples have different phase composition and as expected quite different (inactive, intermediate, and high) photoactivity.

Interestingly, TiO_2 particles have also long been of interest in particle toxicology, where they have largely served as a negative control material in pulmonary studies; however, some systematic evaluations of how particle structure influences biological response have been reported. Several studies found that ultrafine particles of titania are more toxic than equivalent larger fine particles of the same chemical (e.g., TiO_2) composition (Donaldson *et al.*, 1998; Gilmour *et al.*, 1997; Oberdorster, 1996; Oberdorster *et al.*, 1992, 1995). However, titania can exist as several different phases (anatase, rutile, and brookite) and control over this phase in nanoparticle systems is challenging. When produced with grain sizes under ~ 10 nm, titania is generally in the more photoactive anatase form, while larger nanocrystalline titania can be generated as either pure anatase or rutile, or a particularly photoactive mixture of the two (Agrawal *et al.*, 1998; Navrotsky *et al.*, 1967; Zhang and Banfield, 1999). Studies of size-dependent effects in nanoscale titania are thus intrinsically confounded with changes in sample structure and photoactivity. For these reasons, we focus here on the phase composition of nanoscale titania as the primary variable. We hypothesize that this parameter will have the greatest effect on toxicity because it is so strongly correlated with chemical reactivity. Future studies will evaluate what effect, if any, grain size has on the toxicity of nanotitania of constant phase composition.

The studies presented in this manuscript focus specifically on nano-TiO_2 spherical nanoparticles of ~ 3–10 nm diameter (specific surface area [SSA] = 110–155 m^2/g). The high degree of material control afforded by these materials makes it possible to correlate the photocatalytic and *in vitro* toxicological behavior and relate both back to the basic phase composition of nano-TiO_2 particles. We evaluated the photocatalytic properties of various nano-TiO_2 particles (anatase, anatase/rutile, and rutile) and compared these properties with biological endpoints such as cytotoxicity and inflammatory indices of human dermal fibroblasts (HDF) and immortalized human lung epithelial cells (A549). Biological endpoints including lactate dehydrogenase (LDH) release, metabolic activity, and production of inflammation mediators were all evaluated in exposed cells. We found that more photoactive titania materials exhibited more substantial toxicological effects on cells. Both of these results are correlated to the ability for nanotitania to generate RS species, and we confirmed this using *ex vivo* chemiluminescence studies and the degradation of an azo dye. This paper not only shows the photochemical and cytotoxicological differences in the anatase and rutile phases of TiO_2 nanoparticles, but also demonstrates that for these systems *ex vivo* methods for detecting RS species can correlate well with *in vitro* toxicological data.

MATERIALS AND METHODS

Nano-TiO_2 Particle Production

Chemicals. The Degussa Corporation Hanau-Wolfgang, Germany supplied a commercial control anatase/rutile mixture (Degussa TiO_2). Milli-Q ultrapure water (18.2 MΩ cm) was obtained using a Millipore purification system. Titanium (IV) isopropoxide (99.999%), titanium (IV) chloride (99.995%), Congo red (85%), and 2-propanol (99.5%) were purchased from Aldrich (St. Louis, MO); titanium (IV) ethoxide (97%) was obtained from Fluka (Seelze, Germany); dry ethanol (200 proof) was from Pharmco (Brookefield, CT); and hydrochloric acid, sodium hydroxide, and sodium chloride were from Fisher Scientific (Fairlawn, NJ). All chemicals were used "as received" without further purification.

Preparation of nano-TiO_2 anatase particles. Hydrothermal anatase dots were prepared as follows. First, a known amount of ultrapure water was dissolved in dry ethanol and heated with stirring inside a 450-ml Monel autoclave (Parr Instruments, Moline, CA, Model no. 4562). Once the autoclave reached the desired temperature, a solution of titanium (IV) ethoxide ($Ti(OEt)_4$, 0.32 mol/l) in dry ethanol was injected into the reactor. In all cases, the total reaction volume was 100 ml and the molar ratio of water to ethoxide was 20:1. The reaction mixture was stirred at constant temperature for 2 h and then cooled by plunging the vessel in a water bath maintained at room

temperature. The product was filtered, washed twice with water, and air-dried overnight in an oven maintained at 60°C.

Preparation of nano-TiO_2 rutile and nano-TiO_2 anatase/rutile particles. The nano-TiO_2 rutile and anatase/rutile samples were prepared with grain sizes of 3–5 nm using a modified procedure similar to that reported by Cheng *et al.* (1995). For these materials, titanium (IV) chloride ($TiCl_4$, 0.5 mol/l) was added slowly to ultrapure water (450 ml) at room temperature to produce a white suspension of amorphous TiO_2. Hydrochloric acid (37.5%, 50 ml) was added to the suspension as a peptizing agent, and after stirring overnight, the mixture became clear. Then, a 100-ml portion of the peptized TiO_2 suspension was adjusted to the desired pH by addition of aqueous sodium hydroxide, after which it was heated to 85–100°C and refluxed for 2 h. The nanoscale TiO_2 particles were recovered from this solution by the addition of solid sodium chloride, followed by centrifugation. The pellet was washed twice with the ultrapure water and dialyzed (Spectra/Por, membrane molecular weight cutoff = 3500 MW) in several successive ultrapure water baths (4 l each) for a total of at least 24 h to remove unreacted titanium. The resulting powder (100% pure TiO_2) was dried overnight in an oven maintained at 60°C.

Nano-TiO_2 particle sample characterization. All nano-TiO_2 powders were characterized using X-ray diffraction (XRD) (Otwinowski and Minor, 1997), transmission electron microscopy (TEM), Brunauer-Emmett-Teller (BET)–SSA analysis (Brunauer *et al.*, 1938), and differential thermal analysis (DTA) (Kissinger, 1957). XRD patterns were collected using a Siemens Platform-Model General Area Detector Diffraction System with a Cu Kα source. The powder samples were run with an internal silicon powder standard to account for instrumental line broadening when calculating grain sizes from the TiO_2 linewidths. Grain sizes were estimated according to the Debye-Scherrer formula with Warren's correction for instrumental broadening (Klug and Alexander, 1954):

$$D(\text{Å}) = 0.89\lambda/\beta\cos\theta_B,$$

where D is the crystallite size, λ is the X-ray wavelength (1.54 Å for Cu Kα radiation), and θ_B is the Bragg angle. The parameter β is defined as $\beta \equiv (B^2 - b^2)^{1/2}$, where B and b are the linewidths of the most intense TiO_2 reflection ((1 0 1) for anatase and (1 1 0) for rutile) and the (1 1 1) line of the silicon standard, respectively.

BET-SSAs were determined from N_2 adsorption onto the nano-TiO_2 powders using a Micromeritics ASAP 2010 apparatus. Samples were degassed for several hours prior to the N_2 adsorption analysis, which was carried out at liquid nitrogen temperature (− 196°C). Transmission electron micrographs were taken on a JEOL 2010 microscope. Each TEM sample was prepared by flash freezing 2 µl of 3 mg/ml nano-TiO_2 solution via FEI Vitrobot at liquid nitrogen temperature (− 196°C) onto a 300-mesh copper/carbon grid (Ted Pella, Inc., Redding, CA). DTA was performed in air on a Thermal Advantage SDT 2960 apparatus using a temperature range of 25–600°C and a heating rate of 20°C/min.

Before the nano-TiO_2 powder samples were inoculated into the *in vitro* systems, each was suspended in Mill-Q ultrapure water (UVPlus, Millipore, Billerica, MA) at a concentration of 30 mg/ml. Each stock solution was subsequently diluted serially to yield seven concentrations ranging from 3 µg/ml to 30 mg/ml. These samples were then sonicated (Ultrasonic Processor, 50 W/60 Hz) for 30 min before exposure to cells in culture to produce a stable, less aggregated nanocrystalline suspension; typically, solutions were slightly clouded and gave no evidence of settling over the course of the experiment (50 h). All samples were prepared under sterile conditions.

Further analyses of these samples in cell culture media suspensions indicate an increased aggregation state. However, each nano-TiO_2 sample exhibits similar changes in aggregation. Because of this, nanoparticle size is not a variable in these studies.

Cytotoxicity and Inflammation Studies of Nano-TiO_2 Particles on Human Cell Lines

Two cell lines were used in this study. The initial cytotoxicity screen was probed using HDF (Cambrex, Baltimore, MD) cultured in Dulbecco's Modification of Eagle's Media supplemented with 10% fetal bovine serum and 1% L-glutamine, penicillin, and streptomycin. Studies were expanded to include immortalized human lung epithelial cells to monitor the production of inflammation mediators. Human lung epithelial cells (A549) (ATCC, Manassas, VA) were cultured in F-12K media supplemented with 10% fetal bovine serum and 1% L-glutamine, penicillin, and streptomycin. For both cell lines, passage numbers 2–10 were used in the experiments, and cells were seeded at a density of 2×10^5 cells/ml. For these experiments, cells were exposed to uncontrolled ambient light conditions or in one instance, controlled exposure to a nontoxic UV light.

Various biochemical endpoints were examined in this report. For these analyses, all chemicals were purchased from Sigma Aldrich (St. Louis, MO) at the highest purity unless otherwise stated. Tests for LDH release, mitochondrial activity (1-(4,5-dimethylthiazol-2-yl)-3,5-diphenylformazan [MTT]), and production of an inflammatory mediator (interleukin-8 [IL-8]) were performed on both cell lines (HDF and A549) and done in triplicate. The nano-TiO_2 anatase, anatase/rutile, and rutile samples were used in both the cytotoxicity screen and LDH release. The results of these tests showed that the nano-TiO_2 anatase/rutile sample, a 60:40 mixture of anatase and rutile TiO_2, fell between the nano-TiO_2 anatase and rutile biological response. Therefore, the MTT and IL-8 tests were conducted on nano-TiO_2 anatase and rutile samples only. Data are presented as mean ± SD, and an ANOVA followed by a Dunnett's test was used to determine significance. The single factor ANOVA test was applied specifically to the samples used in a particular study as well as each dilution of the sample being tested. Statistical significance was established as $p < 0.05$. All statistical tests were performed with Excel software (Analysis ToolPak for Microsoft Excel 2000).

Live/dead viability screen. To determine the cytotoxic response of the different nano-TiO_2 samples to cells in culture, a viability stain was used to determine dose-response and time-course relationships. First, HDF cells were inoculated with nano-TiO_2 particles (anatase, anatase/rutile, rutile, and Degussa TiO_2) ranging from 0.3 µg/ml to 3 mg/ml for 48 h. Since the nano-TiO_2 samples were in powder form, the exact mass concentrations of the final inoculation solutions were precisely determined (i.e., 3 mg of nano-TiO_2 in 1 ml of ultrapure water). We note that converting these mass doses into a particle number density is problematic due to the distribution in particle sizes. For this reason, we express all doses in terms of mass of particles. Second, cells were exposed to nano-TiO_2 anatase particles and then subsequently stained at varying time points ranging from 1 to 48 h postinoculation. For both experiments, calcein AM (0.5%) and ethidium homodimer (2%) (Molecular Probes, Carlsbad, CA) in phosphate buffer saline (PBS) solution were used to determine cell viability after exposure to nano-TiO_2 anatase and rutile particles (Nolan and Packer, 1974).

LDH release. The release of LDH was monitored in cells dosed with varying concentrations of nano-TiO_2 anatase, anatase/rutile, and rutile particles (3 µg/ml–3mg/ml). Cells (HDF and A549) were seeded in 24-well plates, exposed to nano-TiO_2 particles, and incubated for 48 h. After incubation, the plate was centrifuged at 1900 rpm for 4 min. The media was transferred into a fresh 24-well plate and analyzed for LDH release, as described previously (Decker and Lohmann-Matthes, 1988; Legrand, 1992). Upon addition of assay solutions, the media was protected from the light for 30 min. During this exposure time, Nicotinamide adenine dinucleotide is reduced to Nicotinamide adenine dinucleotide using the LDH that was released in the medium during the 48-h incubation. A total of 150 µl of 1 N HCl was then added to each well to terminate the reduction of NADH. The resulting absorbance was measured at 490 nm.

Mitochondrial activity. The MTT assay (Sigma) was used to evaluate mitochondrial activity (Mossman, 1983). Cells grown in 24-well plates were exposed to varying concentrations of nano-TiO_2 anatase and rutile particles (3 µg/ml–3 mg/ml). After 48 h, 150 µl of MTT (5 mg/ml) was added to each well and incubated for 4 h. Afterward, 850 µl of the MTT solubilization solution (10% Triton X-100 in 0.1 N HCl in anhydrous isopropanol) was added to each well. The resulting formazan crystals were solubilized in acidic

isopropanol and quantified by measuring absorbance at 570 nm. Data were calibrated to the appropriate calibration curve as stated in Sigma protocols.

Production of IL-8. Human IL-8 Enzyme Immunometric Assay Kit (Assay Designs) was used to evaluate the production of the inflammation mediator, IL-8 (Beutler *et al.*, 1985). Cells grown in 24-well plates were exposed to varying concentrations of nano-TiO_2 anatase and rutile particles (3 μg/ml–3 mg/ml). A total of 100 μl of each standard and sample were transferred into different wells in a human IL-8 96-well Microtiter Plate (Assay Designs, Ann Arbor, MI), a plate whose wells are coated with monoclonal antibody specific to human IL-8. After the plate was incubated for 1 h at room temperature, each well was washed with 5% tris-buffered saline solution and tapped upside down to dryness. A total of 100 μl of rabbit polyclonal antibody to human IL-8 was added to each well, incubated for 1 h at room temperature, and washed with 5% tris-buffered saline solution and tapped upside down to dryness. This step was repeated with 100 μl of donkey anti-rabbit IgG conjugated to horseradish peroxidase for 30 min and 100 μl of 3,3′,5,5′ tetramethylbenzidine and hydrogen peroxide for 15 min. A total of 100 μl of 1 N aqueous solution of hydrochloric acid was added to each well and spectroscopically measured at 450 nm. A standard curve composed of varying concentrations of human IL-8 (15–1000 pg/ml) was used to standardize the samples of interest.

Exposure to UV illumination. To further investigate the effects of RS generation by nano-TiO_2, cells were exposed to a nontoxic wavelength of UV light ($\lambda = 356$ nm) at an intensity of 10 mW/cm^2 for 20 min after inoculation by titania. The light used in the exposure was wavelength selective, had no thermal effect, and was photometrically calibrated (DeLong *et al.*, 2005). Cells were then incubated and tested for LDH release as described above.

Ex Vivo Reactive Species Determination

We describe two independent methods for determining the presence of reactive species ($O_2^{\bullet-}$ or $OH^{\bullet}$) in aqueous nanoparticle solutions. First, the chemiluminescence of luminol was used to qualitatively probe the production of RS over 20 min. This method, while not quantitative, does provide an indicator of RS production and is completed in the dark (Arnhold *et al.*, 1991; Hadjimitova *et al.*, 2002). Second, a standard method for evaluating the photocatalytic effectiveness of nano-TiO_2 anatase and rutile suspensions was also used as a measure of RS production, particularly $OH^{\bullet}$. In this test, nano-TiO_2 is used to photodegrade the organic dye, Congo red, and its decay can be followed via absorption spectroscopy and correlated to rate constants for radical production in water (Linsebigler *et al.*, 1995; Ohtani and Nishimoto, 1993).

Luminol (< 99%, Sigma) was prepared using Milli-Q water at 0.140M NaCl, 10.0mM PBS, and adjusted to pH 7.30 (Allen and Loose, 1976; Hallett and Campbell, 1983; Murata, 2002; Pfefferkorn, 1995; Takayama, 2005). The solution was stored in the dark at 4°C. Chemiluminescence intensities were measured with a SpectraMax M2 (Molecular Devices, Sunnyvale, CA). Nano-TiO_2 particles, suspended in water or media, were preincubated and evaluated spectroscopically for 1 min in a final volume of 10.0 μl. A total of 190 μl of the luminol solution was added and changes in the luminescence of the sample were measured. The final concentrations of nano-TiO_2 solution and luminol in the plate wells were 0.150 g/l and 0.126 mol/l, respectively. Chemiluminescence intensities were measured as the peak amplitude in arbitrary units. All experiments were repeated at least three times and performed at room temperature in the absence of light.

Under illumination, nano-TiO_2 anatase and rutile samples generate RS species that can be detected via their degradation of dyes. The nano-TiO_2 anatase, anatase/rutile, and rutile suspensions were stirred individually in the dark for at least 24 h (or 1 h in the case of the Degussa TiO_2 sample) to ensure adsorption equilibrium was established prior to irradiation. Photocatalytic reactions were then carried out inside a Luzchem Model 4-V photoreactor equipped with a magnetic stirrer and 14 UV-A lamps with an emission maximum at $\lambda = 350$ nm. In all cases, the total TiO_2 mass concentration was 1.0 g/l and the total suspension volume was 10.0 ml. Initial Congo red concentrations ranged from 1.0 to 30 mg/l (1.4–33 μmol/l). The disappearance of dye was monitored as a function of irradiation time using the UV-Vis absorbance feature at $\lambda = 496$ nm. Dye concentrations were calculated from the total absorbances of the dye/nano-TiO_2 suspensions after correcting for the contributions of nano-TiO_2 particles to the UV-Vis spectra.

RESULTS

Characterization of Nano-TiO_2 Samples

Nanoscale titania samples of variable composition were produced using quenched hydrothermal reactions (Chemseddine and Mortiz, 1999; Trentler *et al.*, 1999). Figures 1A and 1B show the nano-TiO_2 anatase and anatase/rutile samples used in these studies; although the particles are loosely aggregated, individual nanoparticles are clearly defined (Figs. 1A and 1B). While anatase nanoparticles generally aggregate into spherical assemblies, rutile nanocrystals tend to arrange more compactly into larger, striated structures (Fig. 1C). We note that the Degussa TiO_2 control samples used in this work are reported to be ~ 20 nm in grain size and loosely agglomerated (Bickley *et al.*, 1991; Hurum *et al.*, 2003; Sun and Smirniotis, 2003). BET surface areas ranged from 112 to 153 m^2/g in the nanomaterials studied here. In general, higher surface areas corresponded to smaller average crystallite sizes, except for nano-TiO_2 rutile particles, which despite its extremely fine grain sizes (3.2 nm) exhibited only intermediate surface areas (112 m^2/g) as a result of extensive aggregation (Fig. 1C) (Cheng *et al.*, 1995; Hurum *et al.*, 2003; Kominami *et al.*, 1999).

XRD patterns for the three nano-TiO_2 powders confirm their phase composition (Fig. 1D). Nano-TiO_2 anatase/rutile particles are mixed-phase powders with anatase/rutile mass ratios of approximately 40:60. Small amounts of brookite were also detected in the nano-TiO_2 anatase/rutile sample. DTA was used to evaluate the amorphous content of the TiO_2 samples. None of the DTA profiles exhibited an exothermic peak between 350 and 450°C, thus confirming the complete crystallinity of the powders (Fig. 1E). Our control material, Degussa TiO_2 has an 80:20 ratio of anatase/rutile phases (Hurum *et al.*, 2003). In addition to determining the crystallinity of the nano-TiO_2 samples, XRD patterns were utilized to gather grain size of each sample used in this study. Grain sizes can be deduced from the X-ray peak linewidths, as described above in the experimental section, after corrections for instrumental broadening.

Cytotoxicity and Inflammatory Mediator Results with HDF and A549

The nanoparticle samples were exposed to cells in culture and the viability of the populations measured after various time points; in general, all of the nano-TiO_2 samples were found to be have relatively low toxicity compared to other nanoparticle systems such as fullerenes (Sayes *et al.*, 2004). The flowchart describes the experimental protocol used to

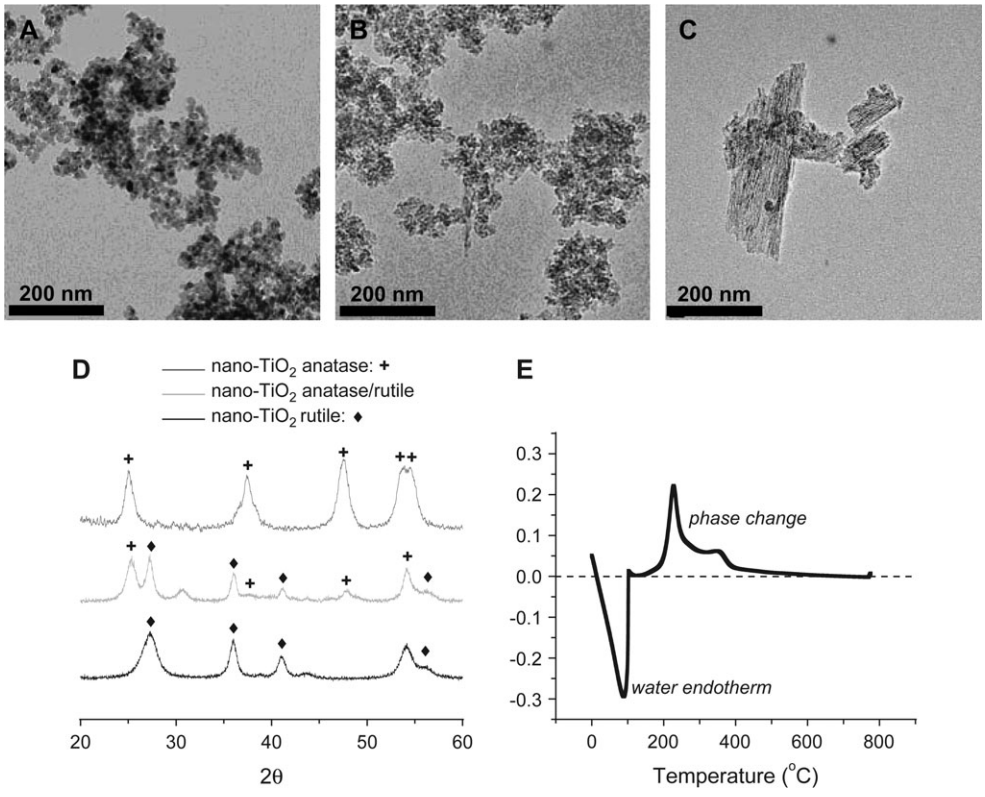

FIG. 1. Characterization data of nano-TiO_2 samples, including TEM images of nano-TiO_2 particles in its (A) anatase, (B) anatase/rutile (60/40), and (C) rutile phases in water. (D) XRD pattern of nano-TiO_2 particles. (E) A representative DTA profile of a nano-TiO_2 photocatalyst. The dip at 100°C corresponds to the removal of water. The peak at 250°C corresponds to the conversion of nano-TiO_2 anatase to nano-TiO_2 rutile. All the samples investigated in the present study exhibited DTA profiles similar to the one shown here.

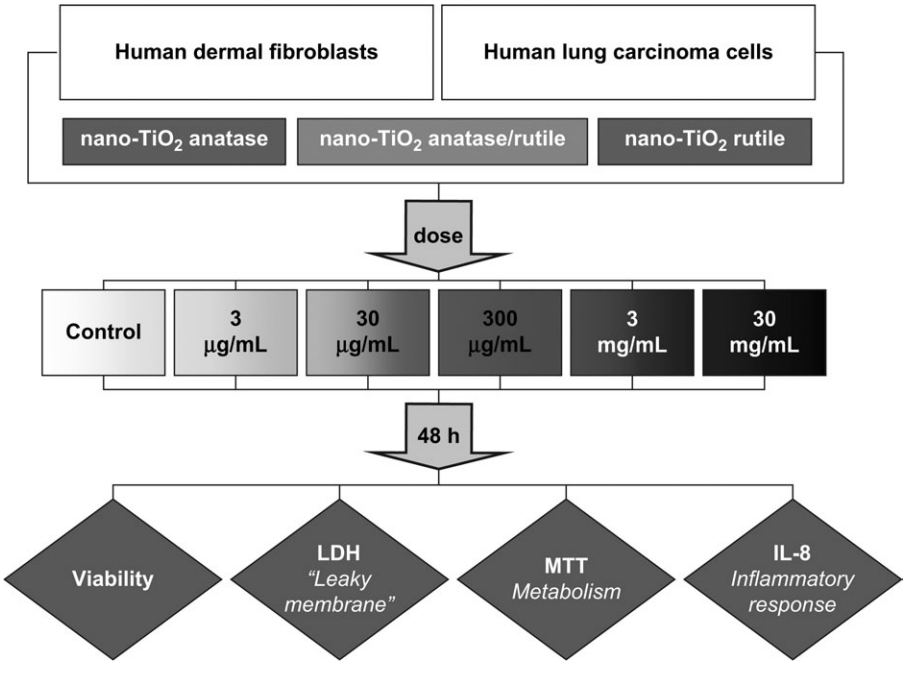

FIG. 2. Flowchart of experimental protocol for testing the cellular response with HDF and A549 cell lines to nano-TiO_2. Cultured cells were dosed with nano-TiO_2 anatase and rutile particles for all experiments and nano-TiO_2 anatase/rutile particles for cell viability experiments. Cells were exposed to nano-TiO_2 particles at various concentrations (3 µg/ml–3 mg/ml), incubated for 48 h, and tested for different biochemical endpoints.

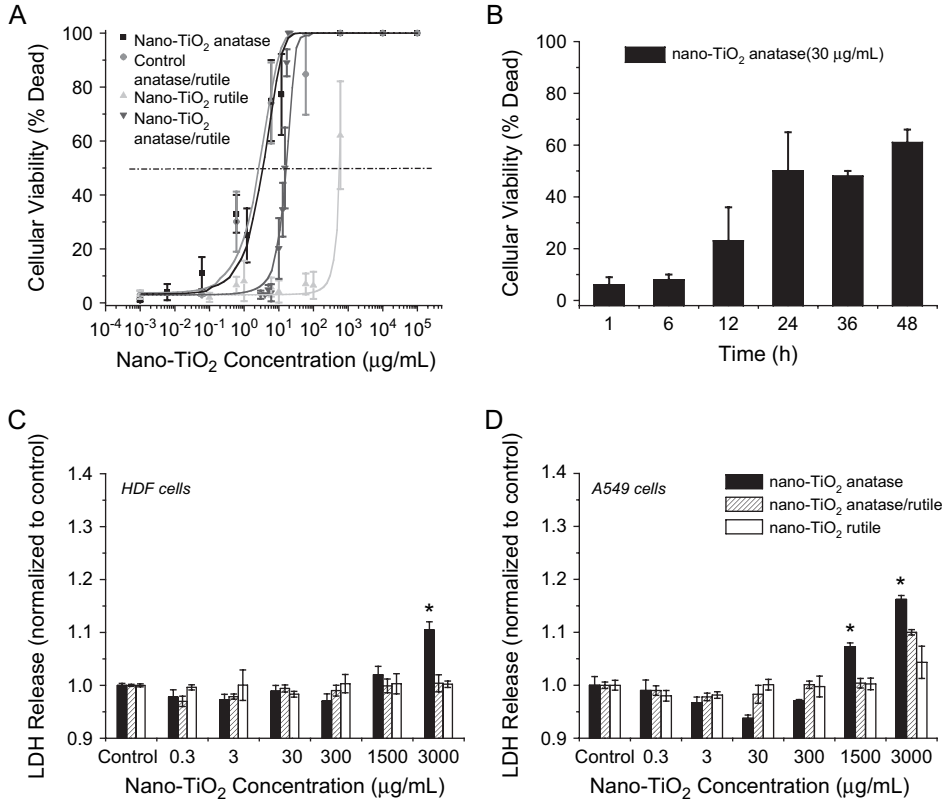

FIG. 3. The dose-response, time-course, and LDH release cellular viability relationships of cultured human cells to nano-TiO_2 samples. (A) Cells were exposed to nano-TiO_2 anatase particles, nano-TiO_2 rutile particles, nano-TiO_2 anatase/rutile particles, and control anatase/rutile (Degussa P25) for 48 h. (B) Cells were exposed to nano-TiO_2 anatase particles and screened at 1 h, 6, 15, 24, 40, and 48 h. LDH release of (C) HDFs and (D) A549 cells after 48 h exposure to nano-TiO_2 anatase, rutile, and anatase/rutile samples. All exposures were done without UV illumination. Results are combined from three independent exposures. Groups significantly different from the control group (by ANOVA $p < 0.00127$ followed by Dunnett's test) are shown by $*p < 0.05$ or $**p < 0.01$.

establish the cellular response of various nano-TiO_2 samples (Fig. 2). Figure 3 shows the dose-response and time-response relationships of various nano-TiO_2 samples on HDFs. The time-response study revealed that the longer the HDFs were exposed to nano-TiO_2 anatase particles, the greater the cytotoxic response (Fig. 3B). The exposure time was truncated at 48 h. At this time point, the cell media lacks sufficient nutrients for cells in culture to remain vital. *Ex vivo* analysis showed that nano-TiO_2 particles stayed in suspension (did not precipitate out of cell culture media) during the course of these experiments.

While overall the toxicity in culture was low, different types of nano-TiO_2 did exhibit different levels of toxicity. Nano-TiO_2 anatase particles were the most cytotoxic to human cells in culture, while nano-TiO_2 rutile particles were the least cytotoxic. Specifically, nano-TiO_2 anatase particles induced an LC_{50} of 3.6 μg/ml, while nano-TiO_2 rutile particles induced an LC_{50} of 550 μg/ml. The control Degussa nano-TiO_2 and another mixed anatase/rutile nano-TiO_2 sample were in between the pure phases in their cytotoxic effect. Additionally, we observed that the toxic response of nano-TiO_2 increased substantially with UV illumination. Figure 4 shows that under UV illumination, cell death increases by 20% ($\lambda = 356$ nm, nontoxic to cells in culture) for a fixed dose.

The observations of cell death in these systems were confirmed by an examination of multiple biochemical endpoints. Figures 4–6 show the results of such studies for both HDF and A549 cells exposed to nano-TiO_2 anatase and rutile particles and anatase/rutile particles for LDH release. Under all conditions, nano-TiO_2 anatase particles produced a greater toxicity, while the nano-TiO_2 rutile sample was the least toxic to the human cells. Specifically, nano-TiO_2 anatase particles produced a high LDH release in cells under ambient conditions and a higher cellular LDH release when exposed to UV light after nano-TiO_2 particle inoculation. Nano-TiO_2 anatase/rutile particles produced a biological response less than that of anatase but greater than rutile. In addition, nano-TiO_2 anatase particles decreased mitochondrial activity (or cellular viability) and enhanced IL-8 in both HDF and A549 cell lines.

Ex Vivo *RS Determination of Nano-TiO_2 Samples*

We sought to correlate the differential cytotoxicity observed in the nano-TiO_2 with the RS production of the same samples.

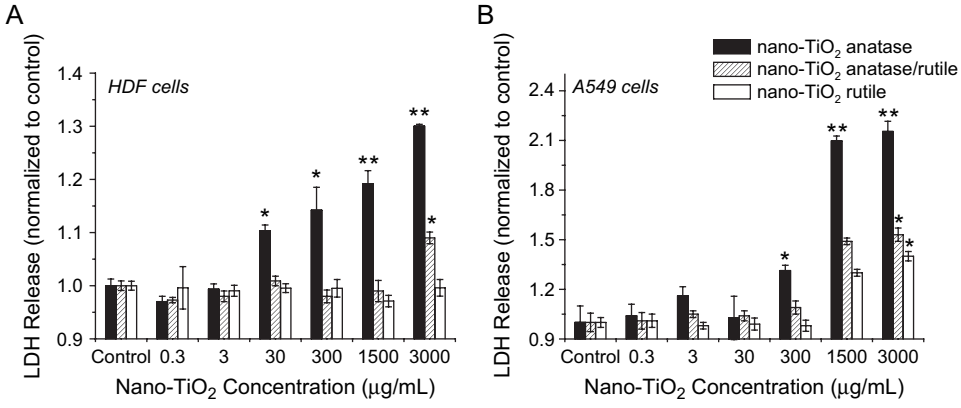

FIG. 4. The LDH release of (A) HDF and (B) A549 cells after 48 h to exposure nano-TiO_2 anatase, anatase/rutile, and rutile samples with a 20-min prior exposure to UV light ($\lambda = 365$ nm, 10 mW/cm^2). Results are combined from three independent exposures. Groups significantly different from the control group (by ANOVA $p_{HDF} < 0.000990$ and $p_{A549} < 0.00211$ followed by Dunnett's test) are shown by $*p < 0.05$ or $**p < 0.01$.

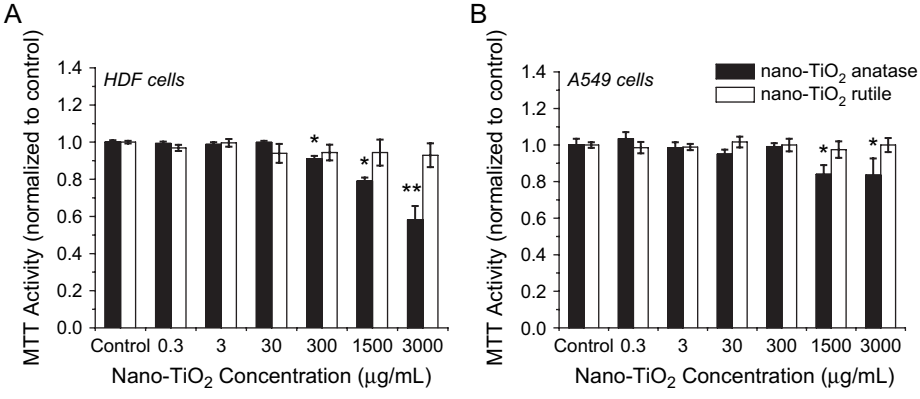

FIG. 5. The mitochondrial activity (MTT activity) of (A) HDF and (B) A549 cells after 48 h exposure to nanoscale TiO_2 anatase and rutile phases. Results are combined from three independent exposures. Groups significantly different from the control group (by ANOVA $p_{HDF} < 0.00231$ and $p_{A549} < 0.00197$ followed by Dunnett's test) are shown by $*p < 0.05$ or $**p < 0.01$).

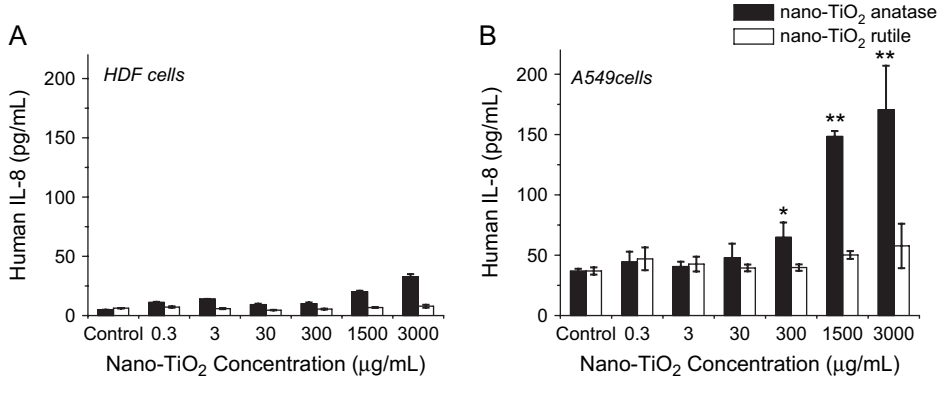

FIG. 6. The production of IL-8 in (A) HDF and (B) A549 cells after 48 h exposure to nanoscale TiO_2 anatase and rutile phases. Results are combined from three independent exposures. Groups significantly different from the control group (by ANOVA $p_{HDF} < 0.0256$ and $p_{A549} < 0.00789$ followed by Dunnett's test) are shown by $*p < 0.05$ or $**p < 0.01$.

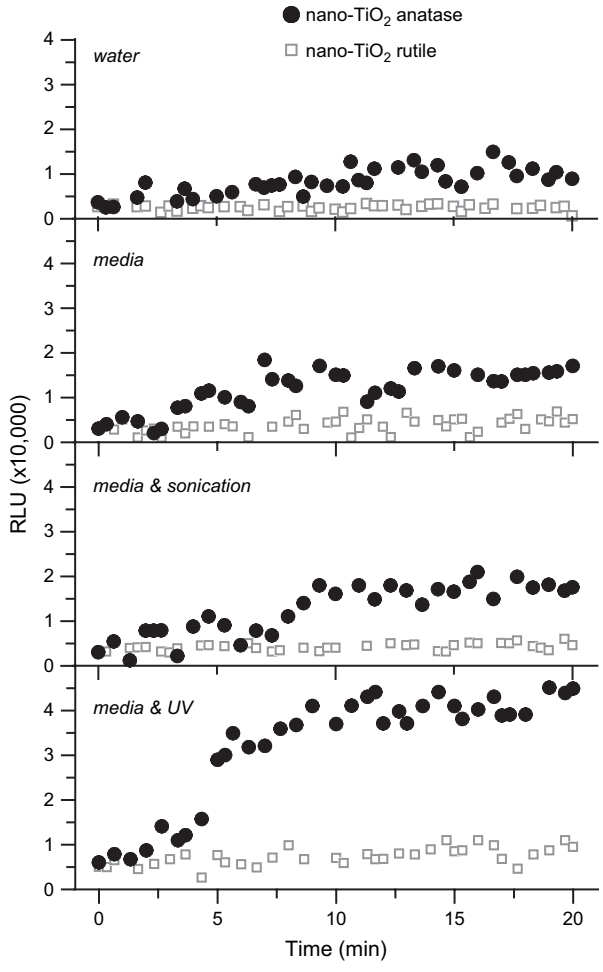

FIG. 7. *Ex vivo* determination of reactive oxygen species in nano-TiO_2 suspensions. The panel shows the emission of light from luminol ($\lambda = 416$ nm) in the presence of nano-TiO_2 anatase particles and nano-TiO_2 rutile particles in (A) water, (B) Dulbecco's Modification of Eagle's Media, (C) media and sonication, and (D) media and UV light. The concentrations of the nano-TiO_2 samples are both 15 mg/ml.

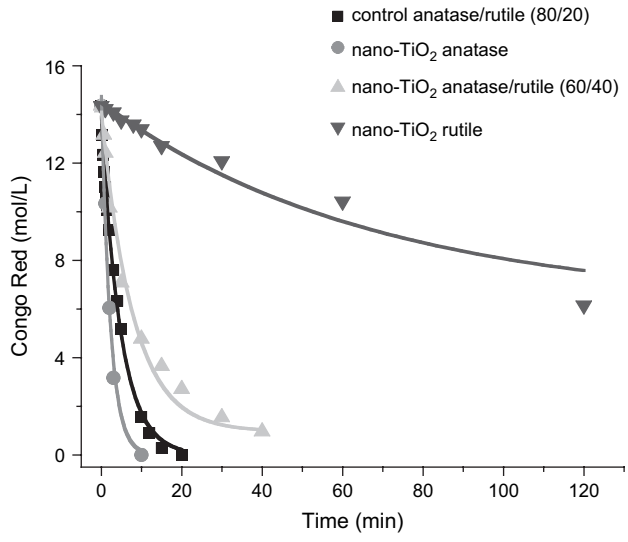

FIG. 8. Photodegradation of aqueous Congo red (10 mg/l, 14 μmol/l) in the presence of various nano-TiO_2 catalysts (1 g/l). Based on this plot, the per gram efficiencies of the TiO_2 powders increased in the order nano-TiO_2 rutile particles < nano-TiO_2 anatase/rutile particles < control anatase/rutile < nano-TiO_2 anatase particles.

Figure 7 shows the *ex vivo* determination of RS in each aqueous suspension of nano-TiO_2 particles using a traditional methodology in biochemistry, namely the chemiluminescence of luminol (Allen and Loose, 1976; Hallett and Campbell, 1983; Murata, 2002; Pfefferkorn, 1995; Takayama, 2005). In this test, nano-TiO_2 anatase and rutile particles were added to luminol solutions; an increase in relative luminescent units within the scatter plot indicates an increase in reactive oxygen species, generally interpreted to consist of $OH^{\bullet}$ radicals. These data show that under a wide variety of conditions (dark/illuminated, sonicated, in biological media), nano-TiO_2 anatase particles produce greater levels of reactive species than nano-TiO_2 rutile particles.

To get a more quantifiable measure of RS generation, these samples were also evaluated for their photocatalytic activity. For this, samples were illuminated by UV light and their RS production measured via the degradation of an azo dye. Figure 8 shows the bleaching over time of a 10 mg/l (14 μmol/l) aqueous Congo red solution in the presence of various nano-TiO_2 powders (mass concentration 1 g/l). The dye decomposition curves indicate that the nano-TiO_2 anatase particles and commercial Degussa TiO_2 catalysts were comparably efficient ($t_{1/2,m} = 1.5$–3.5 min, g) on a mass basis, while the mixed-phase powder nano-TiO_2 anatase/rutile particles took slightly longer ($t_{1/2,m} \equiv 5$ min, g) to degrade the dye. In contrast, the photocatalytic reaction was prohibitively slow ($t_{1/2,m} \cong 120$ min, g) in the presence of the nano-TiO_2 rutile particles. The $t_{1/2}$ values obtained for each sample are listed in tabular form in

TABLE 1
Summary of Characterization Data of Nano-TiO_2 Particles

Particle sample	Shape	Size (nm)	Surface area (m^2/g)	Amorphous content	Aggregation
Nano-TiO_2 anatase particles	Spherical	10.1 ± 1.0	153	None	Mild
Nano-TiO_2 anatase/rutile particles	Spherical	3.2 ± 0.34	112	None	Mild
Nano-TiO_2 rutile particles	Spherical	5.2 ± 0.65	123	None	Severe

TABLE 2
Photocatalytic Activity of Nano-TiO_2 Particles

Particle sample	Anatase/rutile ratios	Surface area (m^2/g)	Average diameter (nm)	Half-life of Congo red by unit mass, $t_{1/2,m}$ (min, g)	Half-life of Congo red by unit surface area, $t_{1/2,s}$ (min, m^2)
Degussa TiO_2	80/20	50	~ 21	3.5	175[a]
Nano-TiO_2 anatase particles	100/0	153	10.1	1.5	230
Nano-TiO_2 anatase/rutile particles	60/40	123	5.2	5.0	1160
Nano-TiO_2 rutile particles	0/100	112	3.2	120	13,400

[a]Hurum *et al.*(2003).

Table 2. The photocatalytic activity of each nano-TiO_2 catalyst was quantified using the half-life ($t_{1/2}$) for a 10-mg/l dye solution. The value of $t_{1/2}$ was expressed on both a unit mass basis ($t_{1/2,m}$) and a unit surface area basis ($t_{1/2,s}$). Activities evaluated on a unit mass basis reflected the influence of surface area on a catalyst's efficiency, while activities expressed on a unit surface area basis (i.e., specific activities) reflected the effects of other physical properties independent of surface area.

DISCUSSION

Nano-TiO_2 particles at high enough concentrations will disrupt the normal activity of cells in culture. Particle exposure caused HDF and immortalized human lung epithelial cells to increase LDH release, decrease mitochondrial activity, and produced increased levels of IL-8 (Figs. 3–6). A classic dose-response curve is observed for cell effects for all sample types studied here, and time course experiments show that the toxicological response increases as expected for a standard toxicant (Fig. 3). We note that the doses required to observe changes in cell function, 1500 μg/ml, are relatively large compared to similar studies of carbon nanoparticles, which found altered cell function at much lower doses (0.02 μg/ml) (Sayes *et al.*, 2004, 2005).

Of most interest in this study was the comparison of the *in vitro* toxicity of different phases of nano-TiO_2; it is clear (Table 1) that the phase of the nano-TiO_2 particles, rather than their SSA, is the most important material parameter for determining toxicity. Nano-TiO_2 anatase particles (SSA = 153 m^2/g) induced a cytotoxic response more than two orders of magnitude larger than nano-TiO_2 rutile particles (SSA = 123 m^2/g). Samples of mixed phase fell in between these two extremes (Table 1). We note that this data does not rule out nanoparticle size as a parameter that can influence toxicity; however, it is far less important than phase composition in the case of titania nanoparticles.

The importance of titania phase composition in biological effects is not unexpected; nanoparticle structure, particularly at surfaces, is central for chemical reactivity generally. For titania, anatase, rutile, and anatase/rutile particles differ substantially in their surface chemistry particularly as it relates to generating reactive oxygen species. First-principles calculations have indicated that water molecules will adsorb dissociatively (i.e., as H^+ and OH^-) to anatase faces but nondissociatively (i.e., as H_2O) to rutile faces (Selloni *et al.*, 1998; Vittadini *et al.*, 1998). When these materials are illuminated with UV light, reactive photocarriers trap to the surface where in anatase systems they encounter Ti-OH species that react to form $OH^{\bullet}$. These are thought to be the primary oxidizing species in photocatalytic oxidation processes; thus, as we show in Figure 7, anatase materials are quite effective at degrading organic dyes when illuminated, while rutile materials are comparatively inactive. The half-life ($t_{1/2,s}$) of an azo dye treated with anatase sample is one to two orders of magnitude shorter than that of the nano-TiO_2 rutile sample. Thus, the generally superior photocatalytic activity of anatase particles is not merely a result of the typically

TABLE 3
Summary of Results

Particle sample	Photoactive (Fig. 8)	Generates RS (Fig. 7)	Produces cytotoxic response LC_{50} (Fig. 3)	Induces LDH release (Figs. 3 and 4)	Decreases MTT activity (Fig. 5)	Produces IL-8 (Fig. 6)
Nano-TiO_2 anatase particles	Yes	Yes	1500 μg/ml	1500 μg/ml (w/o light) 30 μg/ml (w/light)	1500 μg/ml	300 μg/ml
Nano-TiO_2 rutile particles	No	No	N/A	N/A	N/A	N/A

N/A = not applicable; w = with; w/o = without.

larger surface areas found in anatase but rather a result of the fundamental differences between the anatase and rutile surfaces. Specifically, the poor performance of nano-TiO_2 rutile particles suggests that even a moderately high surface area (112 m^2/g) cannot compensate for the inefficient $OH^{\bullet}$ production and low adsorptive affinity that typically limit rutile's efficiency as a photocatalyst.

As Table 1 illustrates, those samples that were the effective photocatalysts were also the most cytotoxic and inflammatory in cell culture. For example, the anatase samples were a hundred times faster at degrading organic dyes and also two orders of magnitude more acutely cytotoxic than rutile samples of comparable surface area. Samples of mixed phase fell in between these two extremes, both in catalytic activity and in biological activity. With only four samples, a quantitative correlation is not possible, but the data do suggest that the photocatalytic efficiency and biological effect of nanoscale titania (Table 2) may stem from a common material feature.

We hypothesized that the ability for titania to generate RS could be the central factor that governs both photreactivity as well as acute cellular toxicity and inflammation. Existing literature has established RS production in aqueous nano-TiO_2 anatase systems (Barnes, 1990; Bast *et al.*, 1991; Cronstein *et al.*, 1992; Dargel, 1992; Doelman and Bast, 1990; Frenkel, 1992; Jaeschke, 1991; Kukreja and Hess, 1992). To develop this further, we looked for evidence of RS species in cells exposed to nanotitania (Cho *et al.*, 2004; Maness *et al.*, 1999; Zheng *et al.*, 2000). We confirmed with the luminol method that even without light, nanoscale titania systems can produce radical species (Fig. 7) under a wide range of conditions. The quantity of RS generated is increased when suspended in cell culture media. It is further increased when irradiated with UV light for 20 min. These *ex vivo* tests are confirmed by biological indicators (LDH release, ''leaky membrane'' visualization) that suggest oxidative damage is involved in the mechanism of cell damage for these experiments. While more work is required to definitively establish the mechanism of biological activity of nanoscale titania, it is apparently similar to that found for cells exposed to nano-C_{60}, a water-soluble colloidal aggregate of pristine fullerenes (Sayes *et al.*, 2004). However, unlike aggregated fullerenes, nano-TiO_2 is capable of disrupting the mitochondrial activity of cells (Sayes *et al.*, 2005). These data suggest that Ti-OH anatase surfaces in the presence of appropriate donors may be reactive enough to oxidatively damage biological species even in the absence of light.

CONCLUSIONS

This study relates the photocatalytic effectiveness of different crystalline phases of nano-TiO_2 particles to their cytotoxic responses in HDF and A549 cells (Table 3). The most inactive catalytic materials (rutile) were two orders of magnitude less cytotoxic than similarly sized anatase nanoparticles that exhibited high photoactivity. This correlation is a manifestation of a fundamental structure-activity relationship in nanoscale titania; nanoparticle structures optimized to produce RS species under UV illumination also are more effective at disrupting cellular functioning. Our data suggest that oxidative damage, whether light induced in photocatalysis studies or generated in biological media, is strongly predicted by the phase of nanoscale materials. Simple *ex vivo* tests of nanotitania photoactivity could thus prove useful as a comparative screen for cytotoxicity in this important class of materials.

ACKNOWLEDGMENTS

We thank Prof. Jane Grande-Allen for use of the SpectraMax M2, Prof. Andreas Luttge for use of the ASAP 2010 BET apparatus, and Dr Wenhua Guo for his assistance with TEM characterization. This research was funded by the Center for Biological and Environmental Nanotechnology (EEC-0118007) and DuPont Haskell Laboratory for Health & Environmental Sciences.

REFERENCES

Agrawal, A., Cizeron, J., and Colvin, V. L. (1998). In-situ high temperature TEM observations of the formation of nanocrystalline TiC from nanocrystalline anatase (TiO_2). *Microsc. Microanal.* **4,** 269–277.

Alivisatos, A. P. (1996). Semiconductor clusters, nanocrystals, and quantum dots. *Science* **271,** 933–937.

Allen, R. C., and Loose, L. D. (1976). Phagocytic activation of a luminol-dependent chemiluminescence in rabbit alveolar and peritoneal macrophages. *Biochem. Biophys. Res. Commun.* **69,** 245–252.

Arnhold, J., Mueller, S., Arnold, K., and Grimm, E. *et al.* (1991). Chemiluminescence intensities and spectra of luminol oxidation by sodium hypochlorite in the presence of hydrogen peroxide. *J. Biolumin. Chemilumin.* **6,** 189–192.

Barnes, P. J. (1990). Reactive oxygen species and airway inflammation. *Free Radic. Biol. Med.* **9,** 235–243.

Bast, A., Haenen, G., and Doelman, C. J. A. (1991). Oxidants and antioxidants—state-of-the-art. *Am. J. Med.* **91,** S2–S13.

Beutler, B., Greenwald, D., Hulmes, J. D., Chang, M., Pan, Y. C., Mathison, J., Ulevitch, R., and Cerami, A. (1985). Identity of tumour necrosis factor and the macrophage-secreted factor cachectin. *Nature* **316,** 552–554.

Bickley, R. I., Gonzalez-Carreno, T., Lees, J. T., Palmisano, L., and Tilley, R. J. (1991). A structural investigation of titanium dioxide photocatalysts. *J. Solid State Chem.* **92,** 178–190.

Brunauer, S., Emmett, P. H., and Teller, E. (1938). Adsorption of gases in multimolecular layers. *J. Am. Chem. Soc.* **60,** 309–319.

Cai, R., Kubota, Y., Shuin, T., Sakai, H., Hashimoto, K., and Fujishima, A. (1992). Induction of cytotoxicity by photoexcited TiO_2 particles. *Cancer Res.* **52,** 2346–2348.

Chang, E., Miller, J. S., Sun, J. T., Yu, W. W., Colvin, V. L., Drezek, R., and West, J. L. (2005). Protease-activated quantum dot probes. *Biochem. Biophys. Res. Commun.* **334,** 1317–1321.

Chemseddine, A., and Mortiz, T. (1999). Nanostructuring titania: Control over nanocrystal structure, size, shape and organization. *Eur. J. Inorg. Chem.* 235–245.

Cheng, H., Ma, J., Zhao, Z., and Qi, L. (1995). Hydrothermal preparation of uniform nanosize rutile and anatase particles. *Chem. Mater.* **7,** 663–671.

Cho, M., Chung, H., Choi, W., and Yoon, J. (2004). Linear correlation between inactivation of E-coli and OH radical concentration in TiO_2 photocatalytic disinfection. *Water Res.* **38,** 1069–1077.

Colvin, V. L. (2003). The potential environmental impact of engineered nanomaterials. *Nat. Biotechnol.* **21,** 1166–1170.

Cronstein, B. N., Levin, R. I., Philips, M., Hirschhorn, R., Abramson, S. B., and Weissmann, G. (1992). Neutrophil adherence to endothelium is enhanced via adenosine-A1-receptors and inhibited via adenosine-A2 receptors. *J. Immunol.* **148,** 2201–2206.

Dargel, R. (1992). Lipid-peroxidation—A common pathogenetic mechanism. *Exp. Toxicol. Pathol.* **44,** 169–181.

Davis, R. J. (1992). Synthesis and characterization of Vpi-5 supported TiO_2 clusters. *Chem. Mater.* **4,** 1410–1415.

Decker, T., and Lohmann-Matthes, M.-L. (1988). A quick and simple method for the quantitation of lactate dehydrogenase release in measurements of cellular cytotoxicity and tumor necrosis factor (TNF) activity. *J. Immunol. Methods* **15,** 61–69.

DeLong, S. A., Moon, J. J., and West, J. L. (2005). Covalently immobilized gradients of bFGF on hydrogel scaffolds for directed cell migration. *Biomaterials* **26,** 3227–3234.

Ding, Z., Lu, G. Q., and Greenfield, P. F. (2000). Role of the crystallite phase of TiO_2 in heterogeneous photocatalysis for phenol oxidation in water. *J. Phys. Chem. B* **104,** 4815–4820.

Doelman, C. J. A., and Bast, A. (1990). Oxygen radicals in lung pathology. *Free Radic. Biol. Med.* **9,** 381–400.

Donaldson, K., Li, X. Y., and MacNee, W. (1998). Ultrafine (nanometre) particle mediated lung injury. *J. Aerosol Sci.* **29,** 553–560.

Fortner, J. D., Lyon, D. Y., Sayes, C. M., Boyd, A. M., Falkner, J. C., Hotze, E. M., Alemany, L. B., Tao, Y. J., Guo, W., Ausman, K. D., *et al.* (2005). C-60 in water: Nanocrystal formation and microbial response. *Environ. Sci. Technol.* **39,** 4307–4316.

Frenkel, K. (1992). Carcinogen-mediated oxidant formation and oxidative DNA damage. *Pharmacol. Ther.* **53,** 127–166.

Gilmour, P., Brown, D. M., Beswick, P. H., Benton, E., MacNee, W., and Donaldson, K. (1997). Surface free radical activity of PM10 and ultrafine titanium dioxide: A unifying factor in their toxicity? *Ann. Occup. Hyg.* **41**(Suppl. 1), 32–38.

Gurr, J. R., Wang, A. S., Chen, C. H., and Jan, K. Y. (2005). Ultrafine titanium dioxide particles in the absence of photoactivation can induce oxidative damage to human bronchial epithelial cells. *Toxicology* **213,** 66–73.

Hadjimitova, V., Traykov, T., Mileva, M., and Ribarov, S. (2002). Effect of some psychotropic drugs on luminol dependent chemiluminescence induced by O_2, OH, HOCl. *Psychotropic Drugs and Chemiluminescence in Model Systems* **57C,** 1066.

Hallett, M. B., and Campbell, A. K. (1983). Two distinct mechanisms for stimulation of oxygen-radical production by polymorphonuclear leucocytes. *Biochem. J.* **216,** 459–465.

Hashimoto, K., Wasada, K., Toukai, N., Kominami, H., and Kera, Y. (2000). Photocatalytic oxidation of nitrogen monoxide over titanium (IV) oxide nanocrystals large size areas. *J. Photochem. Photobiol. A Chem.* **136,** 103–109.

Hirsch, L. R., Stafford, R. J., *et al.* (2003). Nanoshell-mediated near-infrared thermal therapy of tumors under magnetic resonance guidance. *Proc. Natl. Acad. Sci. U.S.A.* **100,** 13549–13554.

Hurum, D. C., Agrios, A. G., Gray, K. A., Rajh, T., and Thurnauer, M. C. (2003). Explaining the enhanced photocatalytic activity of Degussa P25 mixed-phase TiO_2 using EPR. *J. Phys. Chem. B* **107,** 4545–4549.

Hurum, D., Gray, K., Rajh, T., and Thurnauer, M. (2005). Recombination pathways in the Degussa P25 formulation of TiO_2: Surface versus lattice mechanisms. *J. Phys. Chem.* **109,** 977–980.

Jaeschke, H. (1991). Reactive oxygen and ischemia reperfusion injury of the liver. *Chem-Biol. Interact.* **79,** 115–136.

Katari, J. E. B., Colvin, V. L., and Alivisatos, A. P. (1994). X-Ray photoelectron spectroscopy of CdSe nanocrystals with applications to studies of the nanocrystal surface. *J. Phys. Chem.* **98,** 4109.

Kirchner, C., Liedl, T., Kudera, S., Pellegrino, T., Javier, A. M., Gaub, H. E., Stolzle, S., Fertig, N., and Parak, W. J. (2005). Cytotoxicity of colloidal CdSe and CdSe/ZnS nanoparticles. *Nano Lett.* **5,** 331–338.

Kissinger, H. E. (1957). Reaction kinetics in differential thermal analysis. *Anal. Chem.* **29,** 1702–1706.

Klug, H., and Alexander, L. (1954). *X-Ray Diffraction Methods for Polycrystalline and Amorphous Materials.* John Wiley and Sons, New York.

Kominami, H., Kato, J., Murakami, S., Kera, Y., Inoue, M., Inui, T., and Ohtani, B. (1999). Synthesis of titanium (IV) oxide of ultra-high photocatalytic activity: High-temperature hydrolysis of titanium alkoxides with water liberated homogeneously from solvent alcohols. *J. Mol. Catal. A Chem.* **144,** 165–171.

Kukreja, R. C., and Hess, M. L. (1992). The oxygen free-radical system—From equations through membrane-protein interactions to cardiovascular injury and protection. *Cardiovasc. Res.* **26,** 641–655.

Legrand, C. (1992). Lactate dehydrogenase (LDH) activity of the number of dead cells in the medium of cultured eukaryotic cells as marker. *J. Biotechnol.* **25,** 231–243.

Li, Q. W., Luo, G. A., and Feng, J. (2001). Direct electron transfer for heme proteins assembled on nanocrystalline TiO_2 film. *Electroanalysis* **13,** 359–363.

Linsebigler, A. L., Lu, G. Q., and Yates, J. T. (1995). Photocatalysis on TiO_2 surfaces: Principles, mechanisms, and selected results. *Chem. Rev.* **95,** 735–758.

Maness, P. C., Smolinski, S., Blake, D. M., Huang, Z., Wolfrum, E. J., and Jacoby, W. A. (1999). Bactericidal activity of photocatalytic TiO_2 reaction: Toward an understanding of its killing mechanism. *Appl. Environ. Microbiol.* **65,** 4094–4098.

Martin, C. R. (1994). Nanomaterials—A membrane-based synthetic approach. *Science* **266,** 1961–1966.

Mossman, T. (1983). Rapid colorimetric assay for cellular growth and survival: Application to proliferation and cytotoxicity assays. *J. Immunol. Methods* **65,** 55–63.

Murata, H. (2002). Suppressive effect of zearalenone, an estrogenic mycotoxin, on bovine neutrophil chemiluminescence. *Vet. Hum. Toxicol.* **44,** 83–86.

Murray, C. B., Norris, D. J., and Bawendi, M. G. (1993). Synthesis and characterization of nearly monodisperse Cde (E = S, Se, Te) semiconductor nanocrystallites. *J. Am. Chem. Soc.* **115,** 8706–8715.

Navrotsky, A., Jamieson, J. C., and Kleppa, O. J. (1967). Enthalpy of transformation of a high pressure polymorph of titanium dioxide to the rutile modification. *Science* **158,** 388–389.

Nolan, J. S., and Packer, L. (1974). Monolayer culture techniques for normal human diploid fibroblasts. *Methods Enzymol.* **32**(Pt B), 561–568.

Oberdorster, G. (1996). Significance of particle parameters in the evaluation of exposure-dose-response relationships of inhaled particles. *Inhal. Toxicol.* **8,** 73–89.

Oberdorster, G., Ferin, J., Gelein, R., Soderholm, S., and Finkelstein, J. (1992). Role of alveolar macrophage in lung injury: Studies with ultrafine particles. *Environ. Health Perspect.* **97,** 193–199.

Oberdorster, G., Gelein, R., Ferin, J., and Weiss, B. (1995). Association of particulate air pollution and acute mortality: Involvement of ultrafine particles? *Inhal. Toxicol.* **7,** 111–124.

Oberdorster, G., Maynard, A., Donaldson, K., Castranova, V., Fitzpatrick, J., Ausman, K., Carter, J., Karn, B., Kreyling, W., Lai, D., *et al.* (2005). Principles

for characterizing the potential human health effects from exposure to nanomaterials: Elements of a screening strategy. *Part. Fibre Toxicol.* **2,** 1–35.

Ohtani, B., and Nishimoto, S. (1993). Effect of surface adsorptions of aliphatic alcohols and silver ion on the photocatalytic activity of TiO_2 suspended in aqueous solutions. *J. Phys. Chem.* **97,** 920–926.

Otwinowski, Z., and Minor, W. (1997). Processing of x-ray diffraction data collected in oscillation mode. In *Macromolecular Crystallography* (C. W. Carter, R. M. Sweet, Eds.) Pt A, Vol. 276, pp. 307–326. Academic Press Inc., San Diego, CA.

Parkin, I. P., and Palgrave, R. G. (2005). Self-cleaning coatings. *J. Mater. Chem.* **15,** 1689–1695.

Paul, B. K., and Moulik, S. P. (1997). Microemulsions: An overview. *J. Dispersion Sci. Technol.* **18,** 301–367.

Pfefferkorn, L. C. (1995). *J. Biol. Chem.* **270,** 8164–8171.

Rajeshwar, K., de Tacconi, N. R., and Chenthamarakshan, C. R. (2001). Semiconductor-based composite materials: Preparation, properties, and performance. *Chem. Mater.* **13,** 2765–2782.

Sayes, C. M., Fortner, J. D., Lyon, D., Boyd, A. M., Ausman, K. D., Tao, Y. J., Sitharaman, B., Wilson, L. J., West, J. L., and Colvin, V. L. (2004). The differential cytotoxicity of water soluble fullerenes. *Nano Lett.* **4**.

Sayes, C. M., Gobin, A. M., Ausman, K. D., Mendez, J., West. J. L., and Colvin, V. L. (2005). Nano-C60 cytotoxicity is due to lipid peroxidation. *Biomaterials* **26,** 7487–7595.

Selloni, A., Vittadini, A., and Gratzel, M. (1998). The adsorption of small molecules on the TiO_2 anatase (101) surface by first-principles molecular dynamics. *Surf. Sci.* **402–404,** 219–222.

Serpone, N., and Emeline, A. V. (2005). Modelling heterogeneous photocatalysis by metal-oxide nanostructured semiconductor and insulator materials: Factors that affect the activity and selectivity of photocatalysts. *Res. Chem. Intermed.* **31,** 391–432.

Serpone, N., Salinaro, A., *et al.* (2001). Deleterious effects of sunscreen titanium dioxide nanoparticles on DNA. Efforts to limit DNA damage by particle surface modification. *Proc. SPIE* **4258**.

Sun, B., and Smirniotis, P. G. (2003). Interaction of anatase and rutile TiO_2 particles in aqueous photooxidation. *Catal. Today* **88,** 49–59.

Tadros, T. F. (1993). Industrial applications of dispersions. *Adv. Colloid Interface Sci.* **46,** 1–47.

Takayama, H., Shimada, N., Mikami, O., and Murata, H. (2005). Suppressive Effect of Deoxynivalenol, a *Fusarium* Mycotoxin, on Bovine and Porcine Neutrophil Chemiluminescence: An *In Vitro* Study. *J. Vet. Med. Sci.* **67,** 531–533.

Trentler, T. J., Denler, T. E., Bertone, J. F., Agrawal, A., and Colvin, V. L. (1999). Synthesis of TiO_2 nanocrystals by nonhydrolytic solution-based reactions. *J. Am. Chem. Soc.* **121,** 1613–1614.

Uchino, T., Tokunaga, H., Ando, M., and Utsumi, H. (2002). Quantitative determination of OH radical generation and its cytotoxicity induced by TiO_2-UVA treatment. *Toxicol. In Vitro* **16,** 629–635.

Vittadini, A., Selloni, A., Rotzinger, F. P., and Gratzel, M. (1998). Structure and energetics of water adsorbed at TiO_2 anatase (101) and (001) surfaces. *Phys. Rev. Lett.* **81,** 2954–2957.

Vogler, E. A. (1998). Structure and reactivity of water at biomaterial surfaces. *Adv. Colloid Interface Sci.* **74,** 69–117.

Yu, W. W., Falkner, J. C., Yavuz, C. T., and Colvin, V. L. (2004). Synthesis of monodisperse iron oxide nanocrystals by thermal decomposition of iron carboxylate salts. *Chem. Commun.* **20,** 2306–2307.

Zhang, H., and Banfield, J. F. (1999). A new kinetic model for the anatase-to-rutile phase transformation in nanocrystalline material revealing a second order dependence on the number of particles. *Am. Mineral.* **84,** 528–535.

Zheng, H., Maness, P. C., Blake, D. M, Wolfrum, E. J., Smolinski, S. L., and Jacoby, W. A. (2000). Bactericidal mode of titanium dioxide photocatalysis. *J. Photochem. Photobiol. A Chem.* **130,** 163–170.